Volume 12
Number 34
14 September 2024
Pages 8203–8478

Journal of Materials Chemistry B

Materials for biology and medicine

rsc.li/materials-b

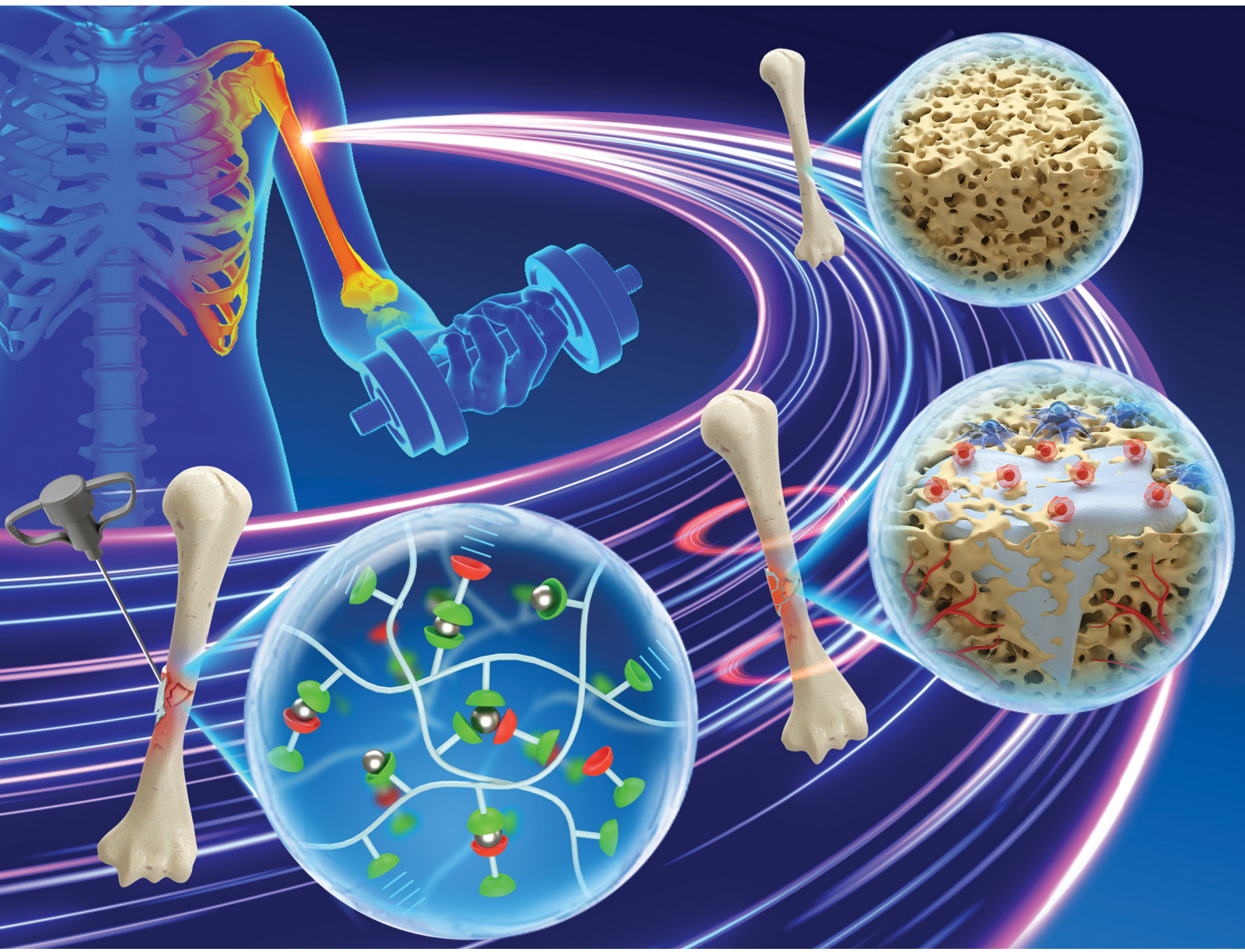

ISSN 2050-750X

ROYAL SOCIETY OF CHEMISTRY

PAPER

Xiao Cen, Jianming Chen, Rong Wang *et al.*
Polyacrylic acid-reinforced organic–inorganic composite bone adhesives with enhanced mechanical properties and controlled degradability

Journal of Materials Chemistry B

ROYAL SOCIETY OF CHEMISTRY

PAPER

View Article Online
View Journal | View Issue

Open Access Article. Published on 25 July 2024. Downloaded on 11/19/2025 6:58:59 AM.
This article is licensed under a Creative Commons Attribution-NonCommercial 3.0 Unported Licence.

Check for updates

Cite this: J. Mater. Chem. B, 2024, 12, 8321

Polyacrylic acid-reinforced organic–inorganic composite bone adhesives with enhanced mechanical properties and controlled degradability†

Pianpian Zheng,‡[abc] Junjie Deng,‡[ab] Lei Jiang,[d] Ning Ni,[d] Xinqi Huang,[e] Zhihe Zhao,[e] Xiaodong Hu,[f] Xiao Cen,*[e] Jianming Chen*[d] and Rong Wang*[abc]

Bone adhesives, as alternatives to traditional bone fracture treatment methods, have great benefits in achieving effective fixation and healing of fractured bones. However, current available bone adhesives have limitations in terms of weak mechanical properties, low adhesion strength, and inappropriate degradability, hindering their clinical applications. The development of bone adhesives with strong mechanical properties, adhesion strength, and appropriate degradability remains a great challenge. In this study, polyacrylic acid was incorporated with tetracalcium phosphate and *O*-phospho-L-serine to form a new bone adhesive *via* coordination and ionic interactions to achieve exceptional mechanical properties, adhesion strength, and degradability. The bone adhesive could achieve an initial adhesion strength of approximately 3.26 MPa and 0.86 MPa on titanium alloys and bones after 15 min of curing, respectively, and it increased to 5.59 MPa and 2.73 MPa, after 24 h of incubation in water or simulated body fluid (SBF). The compressive strength of the adhesive increased from 10.06 MPa to 72.64 MPa over two weeks, which provided sufficient support for the fractured bone. Importantly, the adhesive started to degrade after 6 to 8 weeks of incubation in SBF, which is beneficial to cell ingrowth and the bone healing process. In addition, the bone adhesives exhibited favorable mineralization capability, biocompatibility, and osteogenic activity. *In vivo* experiments showed that it has a better bone-healing effect compared with the traditional polymethyl methacrylate bone cement. These results demonstrate that the bone adhesive has great potential in the treatment of bone fractures.

Received 19th April 2024,
Accepted 24th July 2024

DOI: 10.1039/d4tb00857j

rsc.li/materials-b

1. Introduction

Fractures remain a significant health problem affecting individuals' daily lives.[1] According to a report in 2019, the number of prevalent fractures has reached 455 million globally and continues to increase.[2] Traditional treatment methods, such as the application of plates, intramedullary nails, and screws[3,4] for fixation, carry the risk of secondary injury.[5] Moreover, the handling of fragments resulting from comminuted fractures remains challenging, which further complicates clinical treatment. The utilization of bone adhesives[1,3,6,7] for bone fixation and fragment bonding shows great promise. An ideal bone adhesive material should exhibit good biocompatibility and bioactivity, stimulating new bone formation while degrading at an appropriate rate, thus reducing the risk associated with surgical procedures.

Polymethyl methacrylate (PMMA) is the most common commercially used material for bone fixation.[8,9] However, its monomer is toxic and can release a significant amount of heat during the curing process, leading to potential damage to surrounding tissues. Additionally, the polymer cannot degrade *in vivo*, which can negatively impact tissue regeneration and healing. Other types of bone cement, such as those composed of calcium phosphate and magnesium phosphate, suffer from brittleness, inadequate mechanical strength, and mismatched

[a] Laboratory of Advanced Theranostic Materials and Technology, Ningbo Institute of Materials Technology and Engineering, Chinese Academy of Sciences, Ningbo, 315201, P. R. China. E-mail: rong.wang@nimte.ac.cn
[b] Zhejiang International Scientific and Technological Cooperative Base of Biomedical Materials and Technology, Ningbo Cixi Institute of Biomedical Engineering, Ningbo, 315300, P. R. China
[c] University of Chinese Academy of Sciences, Beijing, 101408, P. R. China
[d] Ningbo No. 6 Hospital, Ningbo, 315042, P. R. China. E-mail: cjmdn01710@163.com
[e] State Key Laboratory of Oral Diseases, National Clinical Research Center for Oral Diseases, West China Hospital of Stomatology, Sichuan University, Chengdu, 610041, P. R. China. E-mail: cenx@scu.edu.cn
[f] Health Science Center, Ningbo University, Ningbo, 315211, P. R. China

† Electronic supplementary information (ESI) available. See DOI: https://doi.org/10.1039/d4tb00857j

‡ P. Zheng and J. Deng contributed equally to this work.

Open Access Article. Published on 25 July 2024. Downloaded on 11/19/2025 6:58:59 AM.
This article is licensed under a Creative Commons Attribution-NonCommercial 3.0 Unported Licence.

degradation rates, thereby limiting their effectiveness in treating fractures. Commercially available medical adhesives, such as fibrin glue,[10,11] have relatively weak bonding strength and are not suitable for providing sufficient support to bone tissue. Cyanoacrylate-based adhesives,[12] on the other hand, exhibit good bonding strength, but their polymerization process generates a significant amount of heat, and their bonding capability on wet tissue surfaces is poor.

Therefore, there is a great need for the development of suitable bone adhesives that can address the limitations of existing materials. One approach is to develop adhesives that combine organic and inorganic components to mimic the structure of bone and achieve optimal osseointegration. For example, Bai and coworkers[13] prepared hydrogel adhesives by co-assembling tannic acid with silk fibroin and hydroxyapatite (HAP), which showed good wet adhesion properties. However, the mechanical strength of these hydrogel adhesives was still weak in terms of load-bearing capacity in practical applications.

To explore bone adhesives with effective strength and biological activities, researchers have turned to biological bonding phenomena observed in nature (such as barnacles, mussels attaching to rocks, spider silk catching insects, *etc.*) for inspiration. It was found that the coordination and ionic bonds[14] between phosphate groups and Ca^{2+} ions are particularly effective in achieving strong bonding on bone surfaces that contain large amounts of calcium salts. Tetracalcium phosphate (TTCP) is a

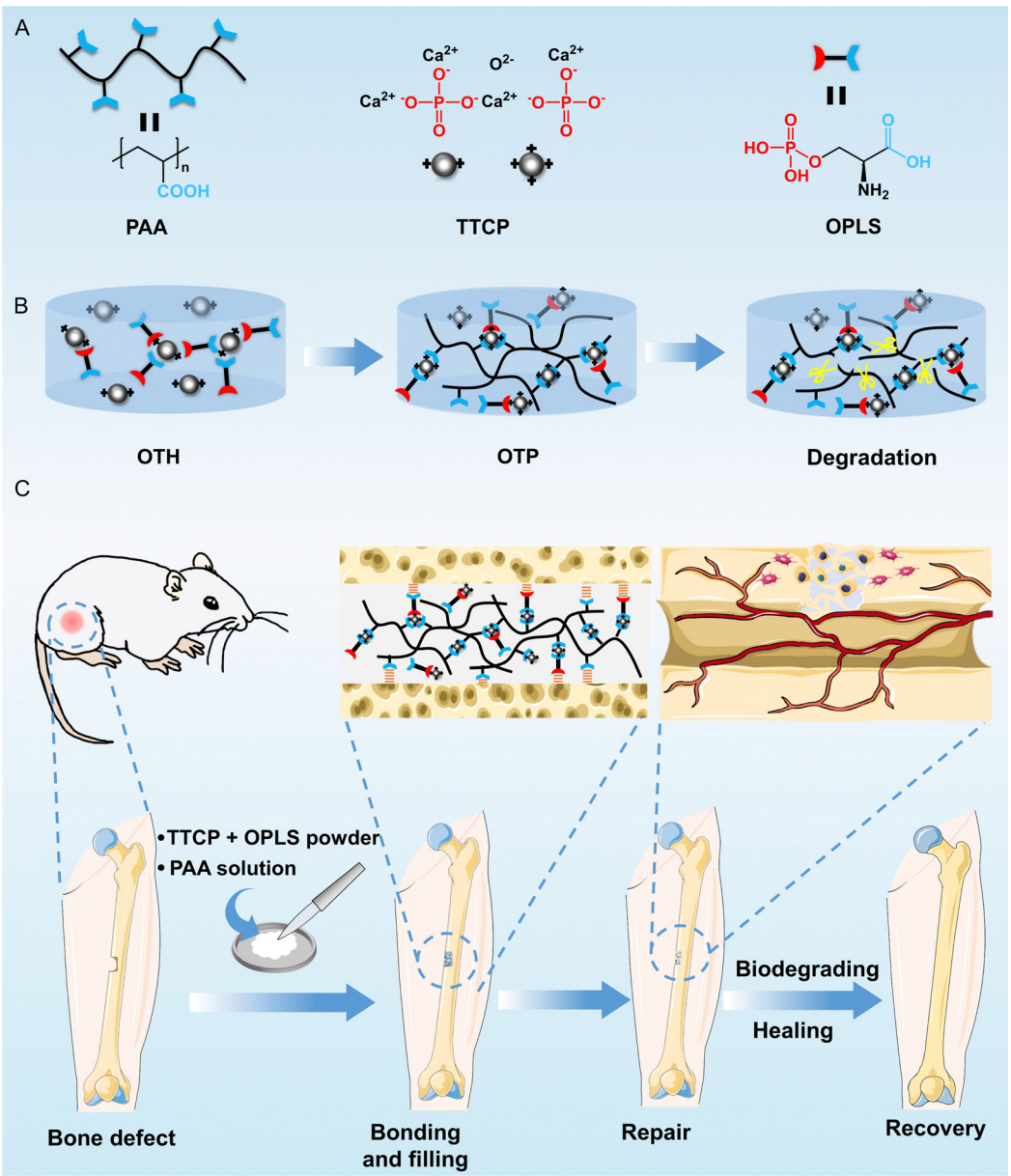

Fig. 1 Schematic illustration of the design of bone adhesives. (A) Composition used for the bone adhesive. (B) The possible mechanism of PAA forms cross-linking structures in bone adhesives (OTH: TTCP and OPLS with water, OTP: TTCP and OPLS with PAA solution) and subsequent degradation. (C) The bonding procedure of bone adhesives, and the healing process of bone fracture with the adhesive applied.

 This journal is © The Royal Society of Chemistry 2024

Open Access Article. Published on 25 July 2024. Downloaded on 11/19/2025 6:58:59 AM. This article is licensed under a Creative Commons Attribution-NonCommercial 3.0 Unported Licence.

basic calcium phosphate[15] and the only calcium phosphate form with a higher calcium–phosphorus ratio than HAP and it has the potential to convert into HAP under conditions with appropriate concentrations of Ca^{2+} and phosphate ions, such as in simulated body fluids (SBF).[16] *O*-Phospho-L-serine (OPLS) is the main component of the sandcastle worm glue[17] and can be well bound with calcium phosphate. Previously, Gall and coworkers developed a bone adhesive based on TTCP and OPLS, and their mechanical strength was enhanced by the addition of poly(lactic-*co*-glycolic acid) (PLGA) fibers and chitosan lactate (CL).[18,19] However, the fiber-filling strategy mainly focuses on changing the physical structure of the adhesive, and the addition of CL does not improve its adhesion properties. In addition, the long-term degradability of bone adhesives, which is crucial for the repair process of bone fractures,[6] has not been fully studied and optimized. Further research is needed to investigate the effect of incorporation of polymers to construct a reinforced network (*via* chemical interactions such as covalent bonds, ionic bonds, *etc.*) in order to improve the mechanical strength, adhesion properties, and degradability of the adhesives.

In this study, various common synthetic and natural polymers were first compounded with TTCP/OPLS adhesives, and their effects on the bonding strength of the adhesives were investigated and compared. It was found that polyacrylic acid (PAA), a synthetic degradable polymer rich in carboxyl groups, is conducive to chelating with metal ions and adhesion to bone tissue through chemical bonding and non-covalent interactions.[20–22] The bonding strength of PAA-incorporated bone adhesive was significantly higher than that of other polymer-incorporated adhesives investigated. The possible mechanisms of the enhancement of the bonding strength were discussed. The adhesive properties, mechanical properties, mineralization ability, biocompatibility, osteogenic activity, and degradability of the adhesive were then thoroughly investigated (Fig. 1A and B). Finally, the bone repair ability of the adhesive was evaluated using a rat model with femoral defects (Fig. 1C).

2. Materials and methods

2.1. Materials

O-Phospho-L-serine (OPLS, >98%) and tetracalcium phosphate (TTCP, 2–20 μm) were purchased from Aladdin (Shanghai, China). Polyacrylic acid (PAA) solution with a molecular weight of 5 kDa and a concentration of 50 wt% was purchased from Macklin (Shanghai, China). PAA solution with a molecular weight of 240 kDa and a concentration of 25 wt% was purchased from Alfa Aesar (Shanghai, China). PAA powder with a molecular weight of 1250 kDa was purchased from Macklin (Shanghai, China). Poly(ethylene glycol) (PEG, molecular weight of 20 kDa), hyaluronic acid (HA), and carboxymethyl chitosan (CMCS) were purchased from Macklin (Shanghai, China). Polyacrylamide (PAM, molecular weight of 10 000 kDa) was purchased from Sinopharm (Shanghai, China). Alginic acid (AA) was purchased from Aladdin (Shanghai, China). Simplex® P bone cement was purchased from Stryker (Beijing, China). Mouse embryonic osteoblast precursor cells (MC3T3-E1) were obtained from Fenghui Biotechnology (Hunan, China). Cell Counting Kit-8 (CCK-8) and Calcein/PI Cell Viability/Cytotoxicity Assay Kit were purchased from Beyotime (Shanghai, China).

2.2. Preparation of bone adhesives

PAA (molecular weight of 5 kDa and 240 kDa) solutions were diluted to a concentration of 25 wt% using deionized water. PEG powder was dissolved in deionized water to a concentration of 25 wt%. PAM, AA, HA, and PAA (molecular weight of 1250 kDa) powders were dissolved in deionized water to a concentration of 1 wt% due to their low solubility. CMCS powder was dissolved in deionized water to a concentration of 5 wt%. Next, 60 mg of OPLS and 100 mg of TTCP were weighed, and 40 μL of deionized water or polymer solution was added to the powder and mixed thoroughly. The mass ratio of OPLS to TTCP was kept at 0.6 according to the literature,[18] and the total liquid-to-solid ratio was 0.25 throughout the study. Finally, the well-mixed paste was applied to the substrate surfaces or injected into a silicone mold for curing in air at room temperature for 15 min, followed by soaking in deionized water at room temperature or SBF at 37 °C for 24 h. The adhesive prepared from OPLS, TTCP, and PAA solution was denoted as OTP, and that prepared from OPLS, TTCP, and deionized water was denoted as OTH.

2.3. Adhesion test on a titanium alloy surface

Cylindrical titanium alloys with a height of 3 cm and a diameter of 1 cm (for the compressive shear test) or 2 cm (for the tensile test) were bonded using OTP or OTH adhesives with the procedure as described above, and cured at room temperature for 15 min, and subsequently soaked in deionized water for 24 h. The compressive shear strength and the tensile strength of the adhesives before and after soaking in deionized water were evaluated using a universal testing machine (CMT-1104). The speed of the universal testing machine was set to 1 mm min^{-1}. For the compressive shear test, the stress–displacement curve was recorded, and the maximum stress observed at the point of failure was considered as the shear strength of the adhesives. For the tensile strength test, the maximum load in the event of adhesion failure was recorded, and the tensile strength was calculated according to eqn (1):

$$P = \frac{4F}{\Pi D^2} \tag{1}$$

where P stands for tensile strength, D is the diameter of the titanium plate (*i.e.*, 2 cm), and F is the maximum tensile force.

2.4. Mechanical properties

Two hundred mg of adhesives were injected into a silicone mold with an internal cavity of 4 mm in height and 6 mm in diameter. After curing in air at room temperature for 15 min and soaking in deionized water for 24 h, the sample was compressed at a speed of 1 mm min^{-1} using a universal testing machine until it was broken. The compressive stress–strain curve was obtained, and the maximum stress value was recorded as the compressive strength of the sample. Additionally, the mechanical stability of the adhesives was assessed by compression testing after the

Open Access Article. Published on 25 July 2024. Downloaded on 11/19/2025 6:58:59 AM. This article is licensed under a Creative Commons Attribution-NonCommercial 3.0 Unported Licence.

samples were incubated in 10 mL of SBF at 37 °C or deionized water at room temperature for up to 14 days. For the tensile test, the adhesive sample was prepared by injecting 800 mg adhesives into a dumbbell-type silicone mold with a thickness of 2 mm and a middle width of 4 mm. After curing in air at room temperature for 15 min and soaking in deionized water for 24 h, the sample was stretched at a rate of 1 mm min^{-1} using a universal testing machine until it was broken.

2.5. pH measurement

Adhesives were fabricated into cylinder samples (4 mm in height and 6 mm in diameter) as described above, and incubated in 2 mL of phosphate-buffered saline (PBS, 10 mM, pH = 7.3) at 37 °C with shaking for up to 7 days. The pH value of the solution was recorded at determined time points.

2.6. *In vitro* hard tissue adhesion test

Pig femurs were bought from a local market and cut into 1 cm × 1 cm × 2 cm cuboid blocks. The two bone blocks were bonded using adhesives or PMMA bone cement. After curing in air for 15 min and soaking in SBF at 37 °C for 24 h, compression shear tests were conducted using a universal testing machine as described above, and the compressive shear strength of the samples was recorded. The premolars were collected at West China Hospital of Stomatology from orthodontic patients with informed consent and approved by the ethical review committee at the West China School of Stomatology, Sichuan University (approval number: WCHSIRB-CT-2024-073). The tooth was cut into two pieces, bonded together using adhesives, and cured in the air for 2 h before testing.

2.7. Curing exothermic measurement

Two hundred mg of adhesives (75 mg of OPLS and 125 mg of TTCP) or PMMA powder were prepared as described above. From the time point of the addition of the liquid component (*i.e.*, PAA solution or deionized water), the temperature of the paste in the curing process over 10 min was recorded using a thermal imager (PI450i, Optris).

2.8. *In vitro* degradation and mineralization test

Two hundred mg of adhesive samples with a size of 4 mm in height and 6 mm in diameter were prepared as described above, and immersed in 10 mL of SBF in a constant shaker at 37 °C. The samples were removed from the solution, dried in an oven, and weighed every week. For observation of structures, the samples were collected and freeze-dried. The surface topography of the samples was observed using scanning electron microscopy (SEM, Regulus 8230, Hitachi) and the internal structure of the samples was analyzed using microcomputed tomography (micro-CT, SKYSCAN 1275, Bruker). The chemical composition of the adhesives was examined *via* X-ray diffraction analysis (XRD, D8 Advance, Bruker), with the 2θ range of 10–80°. The chemical groups of the adhesives were examined using a Fourier transform infrared spectrometer (FTIR, IS 50, Thermo). The scan was performed 32 times within a wavenumber range of 4000 to 400 cm^{-1}. The thermal stability of the adhesives was tested using a thermogravimetric analyzer (TGA, TG209F1, Netzsch) under nitrogen protection, with a set heating rate of 10 °C min^{-1} and a temperature range of 30–1000 °C.

2.9. *In vitro* cell compatibility and proliferation

Mouse embryonic osteoblast precursor cells (MC3T3-E1) were cultured using α-modified Eagle's medium (α-MEM, supplemented with 10% fetal bovine serum and 1% penicillin/streptomycin) at 37 °C in a 5% CO_2 incubator. For preparation of sample extracts, ultraviolet-sterilized adhesives (200 mg) were incubated in 2 mL of α-MEM medium at 37 °C for 24 h or in sterilized deionized water at 37 °C for 7 and 14 days. The resulting extracts were diluted 10-fold with α-MEM medium to obtain the conditioned medium. To investigate the potential toxicity of each component in the adhesive, TTCP, OPLS, and PAA were added to the cell culture medium at the same concentrations as those used in the extracting condition (5 mg mL^{-1}, 3 mg mL^{-1}, and 1 mg mL^{-1}, respectively). MC3T3-E1 cells were seeded in a 96-well plate with 5×10^3 cells per well. After 24 h, the culture medium was replaced with the extract medium or medium containing the testing components and continued for incubation for 1 and 3 days. The medium was replaced with fresh α-MEM medium and an aqueous solution containing 1 wt% of zinc diethyldithiocarbamate as the negative and the positive controls, respectively. The cell viability was determined using CCK-8 assay as per the manufacturer's instructions. For cell morphology and live–dead observation, MC3T3-E1 cells were seeded in 24-well plates at a density of 4×10^4 cells per well. The culture medium was replaced with fresh culture medium or adhesive extracts on the second day. After 3 days of culture, the medium was removed and 250 μL Calcein/PI live–dead staining reagent was added and incubated for 20 min. The cells were then rinsed twice with PBS buffer and observed under an inverted fluorescence microscope (TS2R-FL, Nikon).

For the cell adhesion test, the adhesives were fabricated into thin discs with a diameter of 15 mm and a thickness of 0.5 mm, sterilized by ultraviolet irradiation, and placed in a 6-well plate. Five mL of culture medium was added to each well, and it was incubated at 37 °C for 24 h to fully infiltrate the adhesive sample. After that, the medium was replaced with 5 mL of cell suspension containing 2×10^5 cells in each well. The culture medium was changed after 48 h, and after incubation for 72 h, the adhesive samples were collected. It was rinsed with PBS twice and fixed in 4% paraformaldehyde for 30 min, washed in deionized water twice, and dehydrated in ethanol (25%, 50%, 75%, 90%, 95%, and 100% for 15 min in each step). Finally, the dried samples were sputter-coated with gold, and any cells adhering on the surface were observed using SEM.

2.10. *In vitro* osteogenesis assay

Adhesive samples (1.5 cm in diameter and 0.5 mm in thickness) were placed in 24-well plates, sterilized, and seeded with 1×10^5 MC3T3-E1 cells per well. It was then cultured with differentiation medium consisting of 10% fetal bovine serum, 89% α-MEM, 1% penicillin–streptomycin, 10 nM dexamethasone,

 This journal is © The Royal Society of Chemistry 2024

Open Access Article. Published on 25 July 2024. Downloaded on 11/19/2025 6:58:59 AM.
This article is licensed under a Creative Commons Attribution-NonCommercial 3.0 Unported Licence.

10 mM sodium β-phosphoglycerate, and 50 mg L^{-1} ascorbic acid, with fresh medium replenished every 3 days. Staining was conducted after 3, 7, and 14 days using a BCIP/NBT ALP Chromogenic Kit (Beyotime). Furthermore, the alkaline phosphatase (ALP) activity of the cells was assessed using an alkaline phosphatase (AKP/ALP) activity assay kit (Boxbio Science & Technology), and the absorbance of the cell samples was measured at 510 nm.

The expression of collagen type I (COL1a1) and runt-related transcription factor (RUNX2) osteogenic genes was analyzed by real-time quantitative polymerase chain reaction (RT-qPCR). The adhesive sample (2.5 cm in diameter and 0.5 mm in thickness) was placed in a 6-well plate, co-cultured with MC3T3-E1 cells at a density of 4×10^5 cells per well, and the cells were lysed using TRIzol® reagent (Invitrogen) after 3, 7, and 14 days to extract RNAs. Then, SynScript®III RT SuperMix for the qPCR Kit (Tsingke) was used for reverse transcription amplification, and the obtained cDNA product was diluted 2-fold as a qPCR template, amplified by ArtiCan^{CEO} SYBR qPCR Mix (Tsingke), and the relative mRNA expression of the target gene was counted using the $2^{-\Delta\Delta Ct}$ method. The primer sequences used in this study are listed in Table S1 (ESI†).

2.11. *In vivo* implantation experiments

Male Sprague-Dawley rats (6–8 weeks old, 200–250 g) were used in *in vivo* implantation experiments. All the animal experiments were conducted in accordance with ethical guidelines and were approved by the ethical review committee at the West China School of Stomatology, Sichuan University (approval number: WCHSIRB-D-2023-471). To construct a femur defect in the animal, the rats were anesthetized by inhalation of isoflurane using a portable small animal anesthesia machine (R530, RWD Life Science, Shenzhen, China), and the skin on the surgical region was shaved and disinfected. Then, an oblique incision was made along the rat femur to expose the surgical site. A notch with a size of approximately 5 mm × 3 mm × 1 mm in the middle of the femur was made using an electric grinder, followed by application of ∼50 mg of OTP adhesive or PMMA to the notch site. After that, the muscle and skin were sutured. Each rat was intraperitoneally injected with 100 000 units of penicillin after surgery. After 4 or 8 weeks, the animals were sacrificed and the femur was harvested and analyzed using micro-CT (μCT50, SCANCO, Switzerland).

2.12. Statistical analysis

All data were reported as mean ± standard deviation ($n \geq 3$). A one-way analysis of SPSS program combined with the student *t*-test was used to evaluate the statistical significance of the variance. The differences were considered statistically significant when $p < 0.05$ (ns: non-significant, * $p < 0.05$, ** $p < 0.01$, *** $p < 0.001$).

3. Results and discussion

3.1. Preparation process and adhesion properties of adhesives

The adhesive was prepared by simply mixing TTCP and OPLS powders with a polymer solution to form a homogeneous mixture. The paste-like adhesive then solidified and bonded the adherends together within ∼15 min (a conventional waiting time recommended in the clinic[23]). First, the effects of different polymer solutions on the bonding strength of the adhesives were investigated (Fig. S1, ESI†). The compressive shear strength of the adhesives after adhesion to the titanium alloy and immersion in deionized water at room temperature for 24 h was measured. The result showed that the compressive shear strength of the adhesive was 4.01 MPa without the addition of polymer solution, and increased to 4.61 MPa and 4.68 MPa after the addition of AA and HA, respectively. Furthermore, the compressive shear strength of the adhesive with PAA increased to 5.59 MPa. These results demonstrate that the presence of carboxyl groups has a positive effect on the adhesion properties. However, the adhesion performance of the adhesive with the addition of CMCS added was not improved, probably due to its insufficient content of carboxyl groups. Since bones experience stress in both transverse and longitudinal directions, the adhesion strengths against transverse compressive shear force and longitudinal tensile force were studied (Fig. 2A). The effect of PAA concentration on the performance of the adhesive was then thoroughly investigated (Fig. 2B). As can be seen, the initial compressive shear strength of the adhesive (after curing for 15 min) was 2.97 MPa without the addition of PAA (*i.e.*, OTH adhesive). It decreased slightly to 2.46 MPa after the addition of 2.5 wt% of PAA (molecular weight of 240 kDa). Further increasing the concentration of PAA resulted in an enhancement of the compressive shear strength to 2.65 MPa of 12.5 wt%, and to 3.26 MPa of 25 wt% (the maximum concentration of PAA can be achieved due to the high viscosity of the polymer solution). This could potentially be attributed to the fact that at a low concentration of PAA, which results in partial dissolution of TTCP to produce Ca^{2+}, but the low amount of carboxyl groups cannot undergo sufficient cross-linking with Ca^{2+} ions to form an effective cross-linked structure. As the concentration of PAA increases, the carboxyl groups react and cross-link with Ca^{2+} ions to a higher extent, thereby forming a stable structure and increasing the adhesion strength.

Subsequently, the adhesive was cured in water for a prolonged period to investigate its performance in an aqueous environment, mimicking the *in vivo* conditions (Fig. 2C). Interestingly, the compressive shear strength of the adhesive continued to increase to a maximum value of 5.59 MPa over 24 h, which was higher than the reported values of OPLS/TTCP adhesives reinforced with PLGA and CL,[19] and it remained at this level afterwards. This is probably because PAA requires a longer time for diffusion and to achieve a sufficient cross-linking with TTCP and OPLS. Therefore, as the immersion time increases, the components bind tightly and further cure on the titanium alloy surface, enhancing mechanical interlocking and chemical adhesion. This indicates that the adhesive can maintain good adhesion even in the moist environment of the body, potentially enabling convenient curing during clinical surgery and forming stable adhesion post-operation.

The adhesion performance of the adhesive with PAA of different molecular weights was then investigated (Fig. 2D and E). As can be seen, except for the OTP adhesive with the

Open Access Article. Published on 25 July 2024. Downloaded on 11/19/2025 6:58:59 AM.
This article is licensed under a Creative Commons Attribution-NonCommercial 3.0 Unported Licence.

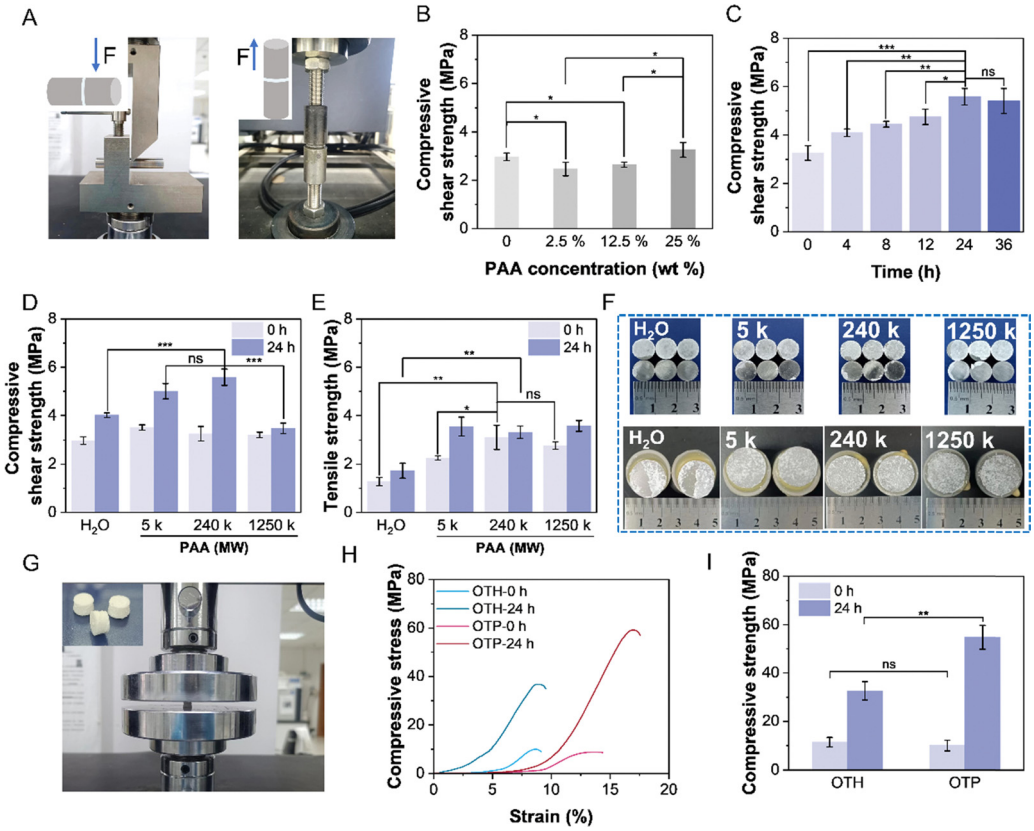

Fig. 2 Mechanical properties of adhesives. (A) Schematic illustration of the compressive shear test (left) and tensile test (right). (B) Compressive shear strength of titanium alloys bonded by adhesives mixed with deionized water or PAA (240 kDa) solution at different concentrations. (C) Compressive shear strength of titanium alloys bonded by the adhesives mixed with 25 wt% PAA (240 kDa) solution, cured in air for 15 min, and soaked in deionized water at room temperature for different periods. (D) Compressive shear strength, and (E) tensile strength of titanium alloys bonded by the adhesives mixed with deionized water or PAA aqueous solutions (25 wt% for PAA with molecular weights of 5 kDa and 240 kDa, or 1 wt% for PAA with a molecular weight of 1250 kDa) before and after soaking in water at room temperature for 24 h. (F) Digital photographs of the titanium alloy surfaces after compressive shear testing (up) and tensile testing (down) showing the failure modes. (G) Digital photograph of the setup for the compression test, with the inset showing the adhesive samples. (H) Compressive stress–strain curves, and (I) strength of the adhesives before and after soaking in water at room temperature for 24 h.

addition of PAA of 1250 kDa, the compressive shear strengths of the other two OTP adhesives (with PAA of 5 kDa and 240 kDa) were higher than that of OTH adhesives (without the addition of PAA) after curing in water for 24 h (Fig. 2D and Fig. S2A, ESI†). The maximum compressive shear strength was achieved by OTP adhesive with the addition of PAA of 240 kDa (5.59 MPa), and it was higher than that of OTP adhesive with the addition of PAA of 5 kDa (5.01 MPa) and PAA of 1250 kDa (3.48 MPa). This difference may be attributed to the shorter molecular chain length of the OTP adhesive with the addition of 5 kDa PAA, in comparison to the OTP adhesive with the addition of 240 kDa PAA, which limits the formation of a robust network structure. On the other hand, OTP adhesive with the addition of 1250 kDa PAA, which was added at a lower concentration of 1 wt% due to its low solubility, might exhibit lower adhesion strength due to the insufficient number of carboxyl groups available for chelation with calcium ions.

The tensile strength of the bonded titanium alloys by the adhesives showed a similar trend (Fig. 2E and Fig. S2B, ESI†), with the maximum strength achieved by the OTP adhesive with the addition of PAA of 240 kDa (*i.e.*, 3.11 MPa after 15 min curing in air and 3.32 MPa after 24 h curing in deionized water). Therefore, PAA of 240 kDa was used in the rest of this study for OTP adhesive preparation. In addition, the failure mode of the adhesive was analyzed (Fig. 2F). As can be seen, the compressive shear test results showed that both OTP and OTH failed in interfacial adhesion, whereas the failure results of the tensile strength test revealed that the OTH adhesive primarily experienced an interfacial adhesion failure. In contrast, the OTP adhesive mainly exhibited a cohesive failure. This indicates that the addition of PAA might enhance the interfacial adhesion and cohesion of the adhesive, possibly due to the interactions between the abundant carboxyl groups in PAA, the metal ions on the titanium surface, and the Ca^{2+} ions in the adhesive. Furthermore, the effect of the addition of PAA on the curing process was also assessed (Fig. S3, ESI†). It was observed that OTH cured and provided sufficient bonding force between two metal columns (200 g each) within 1.5 min, while OTP formed a stable bond after 2 min. This implies that the addition of PAA slows down the curing process of the adhesive, which might be attributed to the addition of PAA hindering the interactions between TTCP and OPLS. Nevertheless, the curing time of OTP is still acceptable in clinical applications.

 This journal is © The Royal Society of Chemistry 2024

Open Access Article. Published on 25 July 2024. Downloaded on 11/19/2025 6:58:59 AM.
This article is licensed under a Creative Commons Attribution-NonCommercial 3.0 Unported Licence.

3.2. Compressive and tensile strengths

In an actual scenario, the bonded bones usually need to bear the load. For this purpose, the bone adhesive itself is required to have sufficient mechanical strength. In this study, the samples were prepared in a cylindrical shape (Fig. 2G) and the compressive strength of OTP and OTH before and after curing in deionized water for 24 h was evaluated (Fig. 2H and I). The results indicated that the OTH and OTP exhibited comparable compressive strengths of 11.39 MPa and 10.06 MPa, respectively, before incubation in water. However, the compressive strength of OTP increased to 54.77 MPa after 24 h of curing in water, compared with that of OTH which only increased to 32.58 MPa after 24 h of curing. This result is aligned with the trend of increasing compressive shear strength (Fig. 2D). In addition, the tensile test (Fig. S4, ESI†) shows that the tensile strength of the OTP was 1.62 MPa after curing in air for 15 min, which was higher than that of OTH (0.78 MPa). After immersion in deionized water for 24 h, the tensile strength of OTH increased to 1.28 MPa, and that of OTP was maintained at a comparable level (1.64 MPa). This trend is aligned with that of the tensile strength in the adhesion test (Fig. 2E) before and after incubation in water. Furthermore, the compressive strength of OTP after 7 and 14 days in SBF at 37 °C and in deionized water at room temperature was measured (Fig. S5, ESI†). The compressive strength of OTP in water increased to 70.94 MPa after 14 days. Moreover, the adhesive showed a compressive strength of 77.69 MPa after 7 days in SBF, and 72.64 MPa after 14 days. To the best of our knowledge, this is the highest value of compressive strength in bone adhesives after prolonged curing reported so far. The adhesive achieves a high compressive strength faster in SBF than in water. This may be because the presence of various ions in SBF facilitates the curing process of the adhesive, leading to a quicker attainment of stable compressive strength. These findings suggest that the adhesive remains mechanically stable for two weeks in a wet environment, exhibiting a certain load-bearing capacity. These results further imply that the addition of PAA enhances the mechanical strength of the adhesive itself, which could be attributed to the COO^- groups from PAA reacting with TTCP and promoting the dissolution of TTCP and formation of a higher amount of Ca^{2+} (Fig. 1B). The resulting Ca^{2+} ions subsequently participate in the ionic cross-linking reactions, facilitating the bridging between PAA chains.[24] Consequently, the bonding between the organic and inorganic components is enhanced, leading to improved cohesion in the adhesive.

3.3. *Ex vivo* hard tissue bonding capacity

The main inorganic component of bone is calcium phosphate. It is expected that the adhesive can bind to Ca^{2+} on the fractured bone surface through ionic and coordination bonds to achieve a strong adhesion effect with the bones. As can be seen, the fractured porcine femur bonded by OTP adhesive after 15 min of curing could withstand a weight of approximately 10 kg (Fig. 3A), and after 2 h of curing, the broken teeth bonded by OTP adhesive could withstand a weight of approximately 5 kg (Fig. 3B). This suggests that the adhesive can

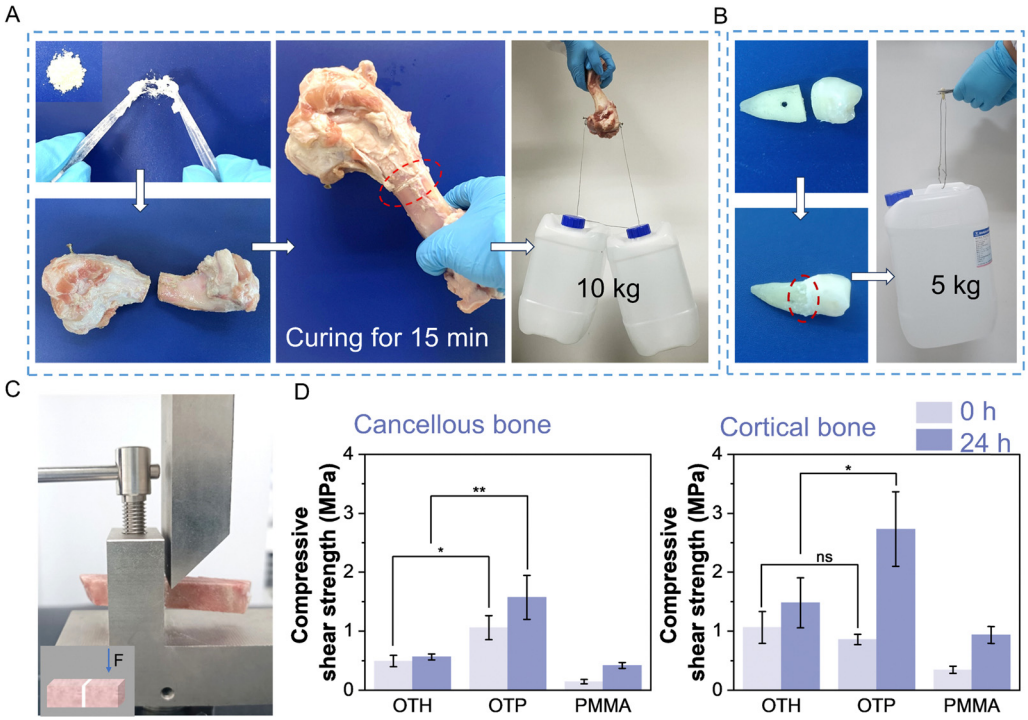

Fig. 3 *Ex vivo* hard tissue bonding capacity. Demonstration of the process of bonding (A) pig femur bones and (B) human tooth with OTP adhesive. (C) Digital photograph and schematical illustration (inset) of the bone adhesion test. (D) Adhesive strength of OTP and OTH adhesives, and PMMA to cancellous and cortical bone before and after soaking in SBF at 37 °C for 24 h.

Open Access Article. Published on 25 July 2024. Downloaded on 11/19/2025 6:58:59 AM.
This article is licensed under a Creative Commons Attribution-NonCommercial 3.0 Unported Licence.

achieve effective adhesion to different hard tissues and is versatile in its applications. To further quantitively measure the adhesion strength, compression shear tests were performed on the porcine femurs (cortical bone and cancellous bone cut into cuboid blocks) using a universal testing machine (Fig. 3C). The results revealed that after undergoing 15 min curing in air, the OTP adhesive displayed an adhesion strength of approximately 1 MPa to both porcine cortical bone and cancellous bone (Fig. 3D). After soaking in SBF for 24 h, the adhesion strength to porcine cancellous bone increased to 1.57 MPa, while that to porcine cortical bone reached 2.73 MPa. Notably, these values were approximately 1 MPa higher than the adhesion strength observed for OTH on bone surfaces. In contrast, the adhesion strength on porcine cancellous bone and cortical bone using PMMA bone cement after soaking in SBF for 24 h was only 0.42 MPa and 0.93 MPa, respectively. These findings

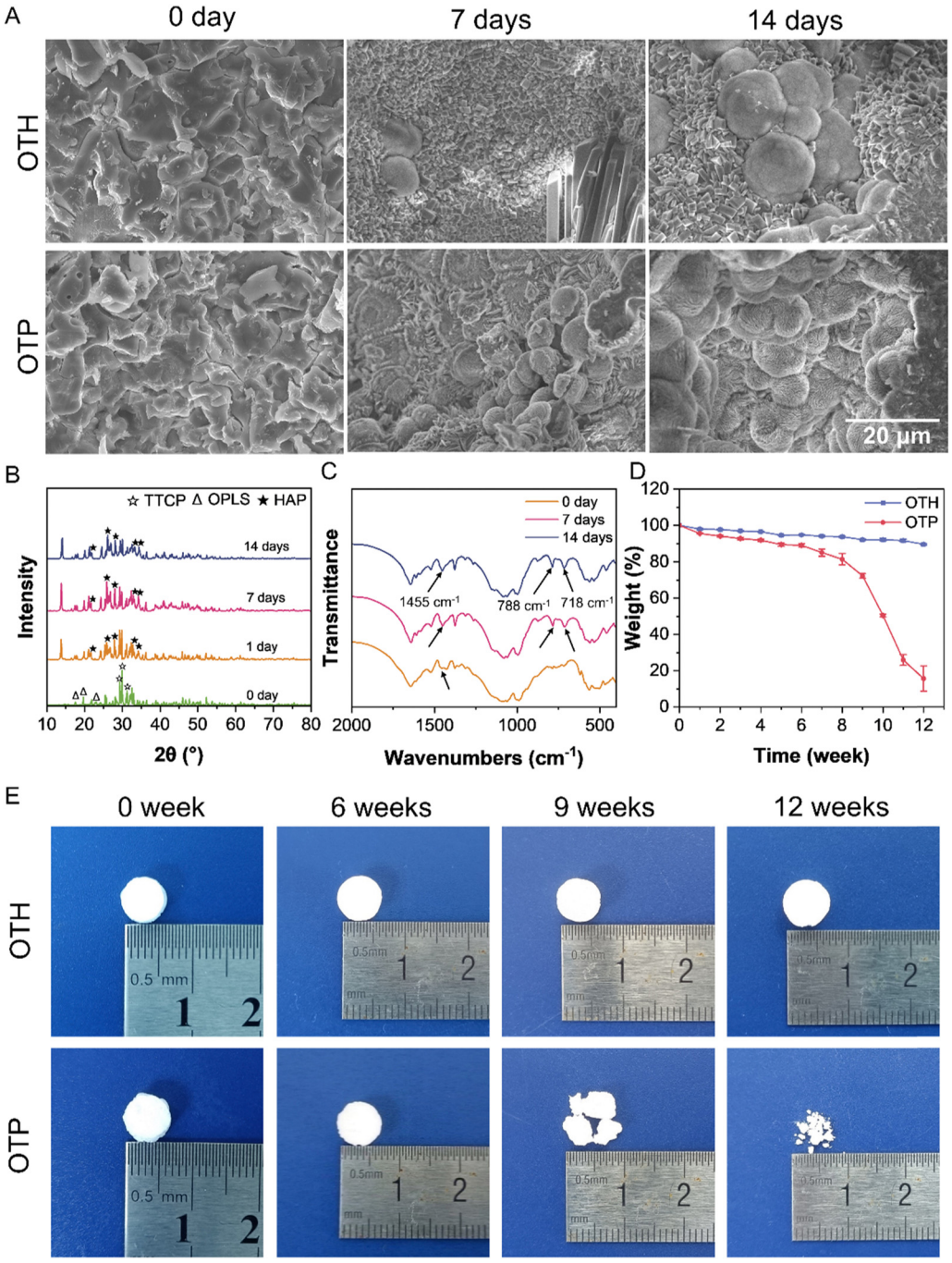

Fig. 4 Mineralization and degradation. (A) SEM images of OTH and OTP adhesives before and after incubation in SBF at 37 °C. (B) XRD and (C) FTIR results of OTP adhesive before and after incubation in SBF at 37 °C. (D) Degradation profile of OTP and OTH adhesives over 12 weeks of incubation in SBF at 37 °C. (E) Digital photographs of OTP and OTH adhesives before and after incubation in SBF at 37 °C for different periods.

 This journal is © The Royal Society of Chemistry 2024

Open Access Article. Published on 25 July 2024. Downloaded on 11/19/2025 6:58:59 AM. This article is licensed under a Creative Commons Attribution-NonCommercial 3.0 Unported Licence.

clearly demonstrate that OTP adhesives possess an excellent hard tissue bonding capability, and they have the potential to bond bones and maintain good adhesion stability in an *in vivo* environment with body fluids.

3.4. Biomineralization and degradability

Since HAP is the primary form of calcium phosphate present in bones, converting the calcium phosphate components in the adhesives into HAP is essential for promoting bone cell growth and, consequently, aiding in the repair of bone fractures.[25,26] To evaluate the mineralization capacity, the adhesives were incubated in SBF at 37 °C over prolonged periods, and the surface morphology was observed using SEM (Fig. 4A). As can be seen, compared with that before incubation (Day 0), HAP was formed on the adhesive surface after 7 days and its amount increased after 14 days. In addition to the globular HAP as shown in Fig. 4A, a thin sheet of HAP with petal morphology, another typical crystalline form of HAP,[27] was also observed (Fig. S6, ESI†). XRD results showed that the intensity of the diffraction peaks belonging to HAP (*i.e.*, 21.7°, 25.9°, 28.0°, 32.9°, and 34.3°) gradually increased, while the main diffraction peak of TTCP (*i.e.*, 29.3°, 29.9°, and 31.2°) decreased after incubation of OTP and OTH in SBF (Fig. 4B and Fig. S7, ESI†), confirming the transformation of calcium phosphate into HAP.

In addition, the TGA and derivative thermal gravimetric curves in Fig. S8 (ESI†) illustrate the decomposition processes of OTP before and after incubation in SBF. Before incubation, the decomposition of OTP could be divided into five stages. The temperature range of 30 °C to 150 °C corresponded to the loss of residual water in the sample. The range of 150 °C to 200 °C represented the decomposition of OPLS. The decomposition of PAA occurred between 200 °C and 360 °C. The broad peak between 360 °C and 540 °C might be attributed to the decomposition of amorphous calcium phosphate formed in OTP. Subsequently, the main decomposition process involved the decomposition of most of the calcium phosphate. The decomposition phase of OPLS in OTP disappeared after 7 and 14 days in SBF, which may be due to its degradation during the long-term incubation. The increase in the decomposition temperature from approximately 410 °C to 500 °C indicates the transition from amorphous calcium phosphate to HAP.[28] The appearance of peaks related to CO_3^{2-} groups (718, 788, and 1455 cm^{-1})[29,30] could be observed in the FTIR spectra of the OTP adhesive after 7 and 14 days of incubation (Fig. 4C), indicating that calcium carbonate also appeared in the OTP adhesive. The presence of HAP and calcium carbonate shows the similarity of the structural composition of the adhesive with that of bone after SBF incubation,[31] and the favorable mineralization capability is conducive to bone cell adhesion and growth.

The bone healing process can be divided into phases of hematoma (inflammation), bone production (soft callus formation), and bone remodeling (hard callus formation).[32] For an ideal bone adhesive, it is required to provide sufficient and stable mechanical support in the hematoma phase, and when the bone production and remodeling phases start, the adhesive should be gradually degraded to allow the ingrowth of cells and the formation of bone structures. An average duration for bone healing ranges from 8 to 16 weeks, and the bone remodeling phase initiates after 3 to 4 weeks of hematoma. Therefore, the bone adhesive must be stable at least until then.[1,4,33,34] The OTP adhesive is stable, and its compressive strength increases to 72.64 MPa after 2 weeks of incubation in SBF (Fig. S5, ESI†). In addition, the *in vitro* degradation behavior of the OTH and OTP adhesives was tested by incubating in SBF over even prolonged periods (Fig. 4D and E). There was no significant change in the size and shape of the OTH and OTP adhesives over 6 weeks of incubation, and the mass loss was less than 10%. However, after 6 weeks, the degradation rate of the OTP adhesive accelerated, causing structural destruction and loss of its original shape. After 12 weeks, only about 15.6% of the OTP adhesive remained, which basically met the degradation needs of fracture healing. In contrast, the OTH adhesive still retained its original shape after 12 weeks, with a mass remaining close to 90%. The slow degradation rate of OTH might adversely affect the healing process of the bone fracture. In addition, the results from micro-CT scanning of the adhesive residuals after degradation showed that OTP had a higher porosity compared to that of OTH after degradation (Fig. S9, ESI†). In sum, the OTP adhesive maintained its mechanical and morphological stability in the early stage of fracture, while PAA was later degraded by hydrolysis, oxidation, and decarboxylation, leading to molecular chain breakage[35–37] (Fig. 1B). In addition, the presence of carboxyl groups in PAA accelerates the dissolution of TTCP, thus releasing more Ca^{2+} that chelates with the carboxyl groups. In the meantime, ion exchange occurs under the action of metal ions (Na^+, K^+, *etc.*) in SBF, promoting the process of Ca^{2+} release.[38,39] The breakage of PAA molecular chains and dissolution of TTCP result in the formation of more pores within the adhesive, thereby accelerating the degradation rate in the later stage and ultimately leading to the gradual destruction of the adhesive as a whole. It should be noted that the test was mainly confined to the *in vitro* environment, and various enzymes and oxidants present in the body will also facilitate the degradation of the adhesives. In conclusion, the OTP adhesive exhibits gradual degradation, thereby allowing cell ingrowth without impeding fracture healing.

3.5. Biocompatibility and osteogenic differentiation

The biocompatibility of adhesive materials intended for bone implantation applications is crucial. However, some traditional acrylate bone cements and adhesives undergo an exothermic reaction during the curing process,[40,41] which can potentially cause damage to bone tissue if the temperature becomes excessively high. The temperature change of OTH and OTP during the curing process was recorded and compared with that of a commercially available PMMA bone cement (Fig. 5A and B). As can be seen, the temperature of OTH and OTP adhesives was kept below 35 °C during the curing process. In contrast, over 10 min of curing, the temperature of the PMMA bone cement reached up to 48 °C, which may cause damage to the bone tissue and lead to thermal necrosis at the site of application.[13] This phenomenon is due to PMMA being cured

Open Access Article. Published on 25 July 2024. Downloaded on 11/19/2025 6:58:59 AM.
This article is licensed under a Creative Commons Attribution-NonCommercial 3.0 Unported Licence.

through a free radical polymerization reaction, which will release a significant amount of heat, while the curing of the OTH and OTP adhesives is mainly the formation of coordination and ionic interactions between the carboxyl groups of PAA, the phosphate groups of OPLS, and the Ca^{2+} of TTCP and bones in a relatively mild process.

Additionally, when the pH of the material significantly deviates from the internal environment of an organism, it can have adverse effects. The pH during the bone repair process undergoes dynamic changes, with the ideal value being around 7.4.[42] Slight alkalinity is beneficial for the deposition of Ca^{2+} and mineralization.[42,43] However, both excessive acidic conditions (pH < 5) and alkaline conditions (pH > 9) disturb the physiological balance and deposition of Ca^{2+} and can result in cell death.[44,45] The influences of OTH and OTP adhesives on the pH of PBS buffer over a prolonged period were investigated (Fig. S10, ESI†). The results showed that the pH of PBS with OTH decreased from 7.30 to 5.70 after 24 h of incubation, and it remained at this level over 7 days. This could be attributed to H^+ released from phosphate and carboxyl groups in OPLS. Similarly, the pH of PBS with OTP decreased to 5.60 after 24 h of incubation and remained stable afterwards. This indicates that the addition of PAA in the OTP adhesive has little effect on the pH of the surrounding environment.

Furthermore, the biocompatibility of the adhesives and their components was evaluated by culture of mouse embryonic osteoblast precursor (*i.e.*, MC3T3-E1) cells. Firstly, TTCP, OPLS, and PAA were added to cell culture medium at the same concentrations as those used for extracting adhesive in medium (5 mg mL^{-1}, 3 mg mL^{-1}, and 1 mg mL^{-1}, respectively). The results showed that after 1 day of co-culture, the cell viability in each of the groups containing the respective component was above 90% (Fig. S11, ESI†), indicating the good biocompatibility of the components used for the adhesives. The live/dead staining of the cells after three days of culturing with the adhesives extract showed that there was no difference in the morphology of MC3T3-E1 cells compared with the control group, and few dead cells were observed in all the groups (Fig. 5C). This demonstrated the excellent biocompatibility of the OTH and OTP adhesives. Interestingly, the quantitative cell viability results showed that both OTH and OTP adhesives had a certain proliferative effect on the cells. The cell viability of the OTP group was about 18% and 21% higher than that of the negative control group (cells were cultured using a normal

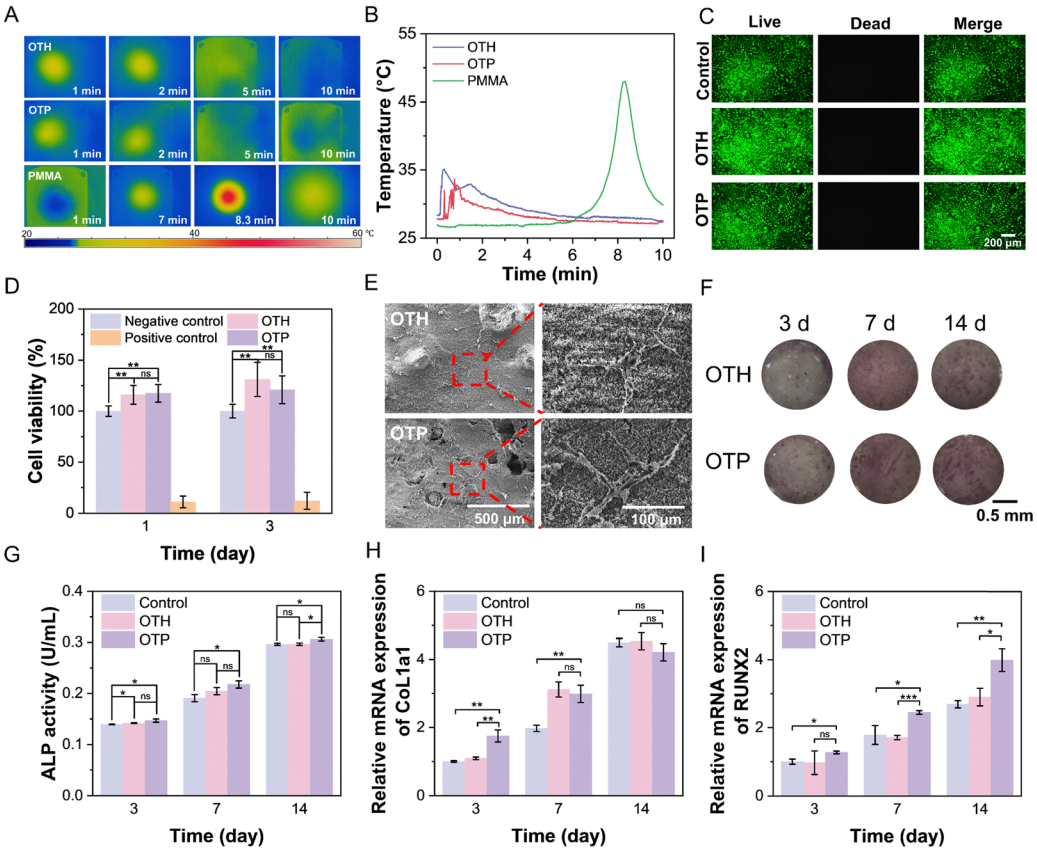

Fig. 5 *In vitro* biocompatibility and osteogenic differentiation. (A) Representative exothermic images, and (B) time-temperature curves of OTH and OTP adhesives, and PMMA during the curing process. (C) Fluorescence microscopic images of the live/dead staining of MC3T3-E1 cells after culture with OTH and OTP extracts for 3 days. Scale bar represents 200 μm. (D) Cell viability of the MC3T3-E1 cells cultured in OTH and OTP extracts for 1 and 3 days. (E) SEM images of MC3T3-E1 cells adhering to OTH and OTP surfaces after 3 days of culture. (F) ALP staining images, and (G) ALP activity of the MC3T3-E1 cells cultured on the surface of OTH and OTP for 3, 7, and 14 days. Gene expression of (H) COL1a1 and (I) RUNX2 in MC3T3-E1 cells cultured on the surface of OTH and OTP for 3, 7, and 14 days.

Open Access Article. Published on 25 July 2024. Downloaded on 11/19/2025 6:58:59 AM.
This article is licensed under a Creative Commons Attribution-NonCommercial 3.0 Unported Licence.

medium that did not contain extracts) after 1 and 3 days, respectively (Fig. 5D). This could be probably attributed to the synergistic effect of Ca^{2+} in TTCP and OPLS that affects the expression of cyclin D1 and cyclin-dependent kinases, and enhances extracellular matrix production,[46–48] resulting in a positive effect on cell proliferation. In addition, the adhesives were incubated in deionized water for 7 and 14 days, and the extracts were co-cultured with MC3T3-E1 cells for 1 and 3 days (Fig. S12, ESI†). The results showed no cytotoxic effects, indicating no toxic substances leached from the fragments or residuals of the adhesives after prolonged incubation. Interestingly, after 3 days of incubation, the extracts from OTP adhesives after 7 days and 14 days of extraction showed an increase of 23% and 15% in cell proliferation, respectively. This is

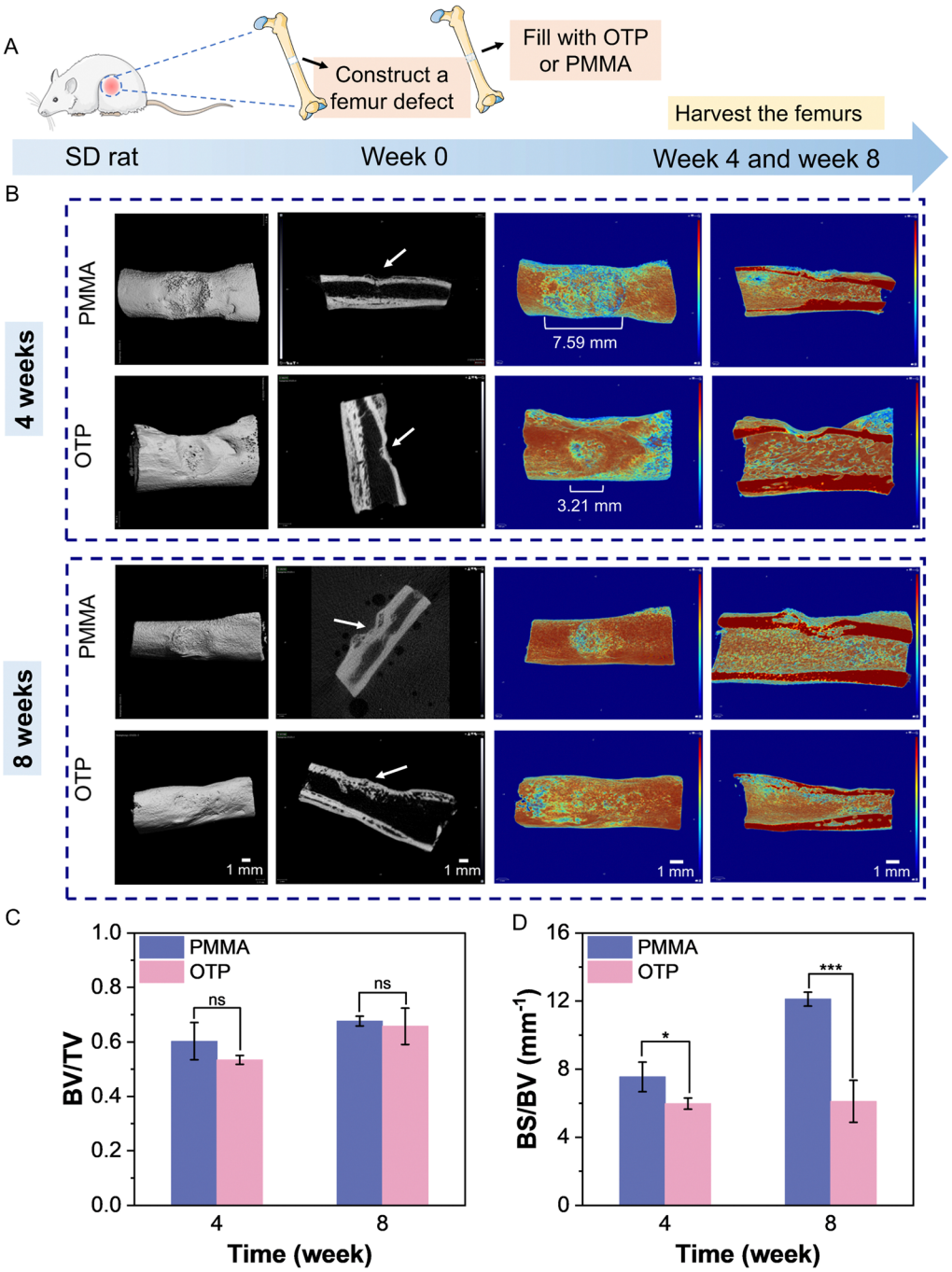

Fig. 6 *In vivo* bone repair evaluation. (A) Schematic illustration of the timeline of the animal experiment. (B) Representative micro-CT images of rat femurs filled with OTP adhesive and PMMA after 4 and 8 weeks. Arrows indicate the bone defect sites. A quantitative analysis of (C) the bone volume fraction (bone volume/total volume, BV/TV) and (D) the bone surface fraction (bone surface/volume, BS/BV) within the notch calculated from the micro-CT data.

Open Access Article. Published on 25 July 2024. Downloaded on 11/19/2025 6:58:59 AM.
This article is licensed under a Creative Commons Attribution-NonCommercial 3.0 Unported Licence.

consistent with the above observations (Fig. 5D), probably due to the enhanced dissolution of TTCP and consequently increased Ca^{2+} release. To further investigate cell growth on the surface of the adhesives, the adhesive was co-cultured with MC3T3-E1 cells for three days, and the cell adhesion was observed using SEM (Fig. 5E). The images revealed that the cells were able to adhere and grow on the adhesive surface, displaying normal cell morphology of MC3T3-E1 cells with elongated and stellate shapes.

Moreover, to assess the *in vitro* osteogenic activity of the adhesive, MC3T3-E1 cells were co-incubated with OTH and OTP adhesive for 3, 7, and 14 days, and their ALP activity was determined. As depicted in Fig. 5F and G, the ALP activity of OTP was slightly higher than that of the OTH group at 14 days. In addition, the expression of osteogenesis-related genes (type I collagen (COL1a1) and runt-associated transcription factor 2 (RUNX2)) in MC3T3-E1 cells after 3, 7, and 14 days of co-incubation with OTH and OTP adhesive was investigated using RT-qPCR (Fig. 5H and I). The elevated expression of COL1a1 is widely regarded as indicative of promoted osteoblast activity and bone matrix synthesis.[49] Upregulation of RUNX2 expression is often viewed as a hallmark that accelerates the process of osteogenic differentiation.[50,51] The results indicated that the expression of COL1a1 in MC3T3-E1 cells cultured with OTP was higher than that in the OTH group after 3 days of incubation, with no significant difference observed in the later stages. RUNX2 expression in cells co-cultured with OTP surpassed that in the OTH group at 7 and 14 days. Overall, OTP demonstrated a higher inclination to foster osteogenic differentiation compared to OTH.

3.6. *In vivo* bone repair capability

To assess the bone repair of the adhesive *in vivo*, an incision was made on the femoral bone of a rat, and OTP adhesive or PMMA was applied to the defect (Fig. 6A). Bone samples were harvested after 4 and 8 weeks, respectively. Micro-CT scans were performed at the surgical site of the rat's femoral bone. The results of 3D reconstruction showed that new bone formed in the surgical site of both the OTP and PMMA groups (Fig. 6B). However, the bone mineral density images of the PMMA group showed a significantly larger area with lower bone density on the surface of the rats' femur compared with the OTP group after 4 weeks of surgery. The width was greater than the size of the incision in the surgery (*i.e.*, 3 mm), indicating possible damage to the surrounding bone tissue caused by the exothermic reaction of PMMA. The quantification results revealed that the ratio of bone volume to total volume (*i.e.*, BV/TV) in the OTP group was 0.53 at 4 weeks and increased to 0.66 at 8 weeks (Fig. 6C). There was no significant difference compared with that of the PMMA group. The ratio of bone surface area to bone volume (*i.e.*, BS/BV) in the OTP group was 5.98 mm^{-1} at 4 weeks and increased to 6.11 mm^{-1} at 8 weeks (Fig. 6D). In contrast, the PMMA group increased from 7.54 mm^{-1} to 12.11 mm^{-1}, which was significantly higher than that of the OTP group. This indicates that new bone maturation is higher in the OTP group and the proportion of cortical bone is larger. In sum, these preliminary *in vivo* results indicate that OTP adhesive has good bone healing capability compared with PMMA bone cement, and it shows great potential for bone surgery applications.

4. Conclusion

In this work, bone adhesives with excellent mechanical properties, adhesion properties, and suitable degradability were prepared by the incorporation of PAA into TTCP/OPLS. The adhesion performance of the adhesives was enhanced by optimization of the concentration and molecular weight of PAA. Thanks to the coordination and ionic interactions between the carboxyl group of PAA, the phosphate group of OPLS, and Ca^{2+} in TTCP, the OTP adhesive exhibited good adhesion to titanium alloys, bones, and teeth. In addition, the adhesion strength could be further improved after incubation in an SBF environment, demonstrating its exceptional wet adhesion ability. The adhesive remains mechanically stable for at least two weeks in a wet environment, exhibiting a prolonged load-bearing capacity. After 6 to 8 weeks, the OTP adhesive started to degrade, which potentially allowed cell ingrowth and bone regeneration at the fracture site. The OTP adhesive also exhibits remarkable mineralization capability, good biocompatibility, and osteogenic activity. Finally, a preliminary *in vivo* study using a rat femoral bone defect model showed that OTP adhesive had good bone repair ability. These results indicate that OTP has great potential for bone surgery applications in the clinic. However, further research on a comprehensive investigation using large animals for the *in vivo* performance of prolonged safety and load-bearing effects should be conducted before the adhesives are translated for clinic applications.

Author contributions

Pianpian Zheng: conceptualization, data curation, formal analysis, investigation, methodology, writing – original draft. Junjie Deng: conceptualization, data curation, investigation, methodology. Lei Jiang: methodology. Ning Ni: methodology. Xinqi Huang: investigation. Zhihe Zhao: investigation, supervision. Xiaodong Hu: methodology. Xiao Cen: methodology, supervision, writing – review & editing. Jianming Chen: methodology, supervision, project administration. Rong Wang: conceptualization, methodology, supervision, writing – review & editing, project administration, funding acquisition.

Data availability

The data sets used to generate the results in this work are available at **https://dataspace.nimte.ac.cn:8080/space/1524644026781818880/details/filesManage**.

Conflicts of interest

The authors declare no conflicts of interest.

 This journal is © The Royal Society of Chemistry 2024

Open Access Article. Published on 25 July 2024. Downloaded on 11/19/2025 6:58:59 AM.
This article is licensed under a Creative Commons Attribution-NonCommercial 3.0 Unported Licence.

Acknowledgements

This work was funded by the Key Research and Development Program of Ningbo (2022Z132), Youth Innovation Promotion Association CAS (2021296), the National Natural Science Foundation of China (32271416), the Sichuan Science and Technology Program (2023NSFSC1521), the Foundation of Director of Ningbo Institute of Materials Technology and Engineering CAS (2021SZKY0301), and Research Funding from West China School/Hospital of Stomatology Sichuan University (RCDWJS2023-17).

References

1 M. Shokri, F. Dalili, M. Kharaziha, M. Baghaban Eslaminejad and H. Ahmadi Tafti, *Adv. Colloid Interface Sci.*, 2022, **305**, 102706.
2 J. A. Cauley, *Lancet Healthy Longevity*, 2021, **2**, e535–e536.
3 M. Zhang, J. Liu, T. Zhu, H. Le, X. Wang, J. Guo, G. Liu and J. Ding, *ACS Appl. Mater. Interfaces*, 2022, **14**, 1–19.
4 M. J. Sánchez-Fernández, H. Hammoudeh, R. P. Félix Lanao, M. Van Erk, J. C. M. Van Hest and S. C. G. Leeuwenburgh, *Adv. Mater. Interfaces*, 2019, **6**, 1802021.
5 Z. Ma, B. Liu, S. Li, X. Wang, J. Li, J. Yang, S. Tian, C. Wu and D. Zhao, *Regener. Biomater.*, 2023, **10**, rbad003.
6 Z. Bao, R. Yang, B. Chen and S. Luan, *Fundam. Res.*, 2024, DOI: 10.1016/j.fmre.2023.11.023.
7 H. B. Bingol, J. C. M. E. Bender, J. A. Opsteen and S. C. G. Leeuwenburgh, *Mater. Today Bio*, 2023, **19**, 100599.
8 L. Chen, Y. Tang, K. Zhao, J. Liu, H. Bai and Z. Wu, *Colloids Surf., B*, 2020, **189**, 110848.
9 F. Banche-Niclot, I. Corvaglia, C. Cavalera, E. Boggio, C. L. Gigliotti, U. Dianzani, A. Tzagiollari, N. Dunne, A. Manca, S. Fiorilli and C. Vitale-Brovarone, *Biomolecules*, 2023, **13**, 94.
10 D. Trucco, L. Riacci, L. Vannozzi, C. Manferdini, L. Arrico, E. Gabusi, G. Lisignoli and L. Ricotti, *Macromol. Biosci.*, 2022, **22**, 2200096.
11 M. Grosjean, E. Girard, A. Bethry, G. Chagnon, X. Garric and B. Nottelet, *Biomacromolecules*, 2023, **24**, 4430–4443.
12 K. Xu, X. Wu, X. Zhang and M. Xing, *Burns Trauma*, 2022, 10.
13 S. Bai, X. Zhang, X. Lv, M. Zhang, X. Huang, Y. Shi, C. Lu, J. Song and H. Yang, *Adv. Funct. Mater.*, 2020, **30**, 1908381.
14 Z. Xiao, Q. Li, H. Liu, Q. Zhao, Y. Niu and D. Zhao, *Eur. Polym. J.*, 2022, **173**, 111277.
15 M. S. J. Anthraper, A. Chandramouli, S. Srinivasan and J. Rangasamy, *Int. J. Biol. Macromol.*, 2024, **258**, 129086.
16 B. Yilmaz, A. E. Pazarceviren, A. Tezcaner and Z. Evis, *Microchem. J.*, 2020, **155**, 104713.
17 H. Shao, K. N. Bachus and R. J. Stewart, *Macromol. Biosci.*, 2009, **9**, 464–471.
18 A. Kirillova, C. Kelly, N. Von Windheim and K. Gall, *Adv. Healthcare Mater.*, 2018, **7**, 1800467.
19 A. Kirillova, O. Nillissen, S. Liu, C. Kelly and K. Gall, *Adv. Healthcare Mater.*, 2021, **10**, 2001058.
20 H. Yuk, C. E. Varela, C. S. Nabzdyk, X. Mao, R. F. Padera, E. T. Roche and X. Zhao, *Nature*, 2019, **575**, 169–174.
21 L. Yan, T. Zhou, R. Ni, Z. Jia, Y. Jiang, T. Guo, K. Wang, X. Chen, L. Han and X. Lu, *ACS Appl. Bio Mater.*, 2022, **5**, 4366–4377.
22 L. Wang, L. Duan, G. Liu, J. Sun, M. A. Shahbazi, S. C. Kundu, R. L. Reis, B. Xiao and X. Yang, *Adv. Sci.*, 2023, **10**, 2207352.
23 Q. Li, B. Tang, X. Liu, B. Chen, X. Wang, H. Xiao and Z. Zheng, *Adv. Healthcare Mater.*, 2024, 2301870.
24 A. O. Majekodunmi and S. Deb, *J. Mater. Sci.: Mater. Med.*, 2007, **18**, 1883–1888.
25 B. Xu, P. Zheng, F. Gao, W. Wang, H. Zhang, X. Zhang, X. Feng and W. Liu, *Adv. Funct. Mater.*, 2017, **27**, 1604327.
26 X. Liu, Y. Zhang, Z. Hussain, P. Zheng, M. Xu, H. Zhao, Y. Liu, Y. Cao, I. Ullah, A. Osaka and R. Pei, *Appl. Mater. Today*, 2023, **30**, 101693.
27 B. Jiang, X. Li, B. Yang, S. Yang, X. Chen, J. Chen, M. Fang, Z. Huang, X. Min and X. Hu, *Appl. Sci.*, 2023, **13**, 11593.
28 S.-S. Jee, T. T. Thula and L. B. Gower, *Acta Biomater.*, 2010, **6**, 3676–3686.
29 G. Yuan, X. Chen, X. Li, Q. Liang, G. Miao and B. Yuan, *Powder Technol.*, 2015, **284**, 253–256.
30 J. Liu, F. Qiu, Y. Zou, Z. Zhang, A. Wang and Y. Zhang, *Ceram. Int.*, 2023, **49**, 20315–20325.
31 V. Sharma, A. Srinivasan, F. Nikolajeff and S. Kumar, *Acta Biomater.*, 2021, **120**, 20–37.
32 A. Tzagiollari, H. O. McCarthy, T. J. Levingstone and N. J. Dunne, *Bioengineering*, 2022, **9**, 250.
33 R. Marsell and T. A. Einhorn, *Injury*, 2011, **42**, 551–555.
34 D. J. Hadjidakis and I. I. Androulakis, *Ann. N. Y. Acad. Sci.*, 2006, **1092**, 385–396.
35 H. Arkaban, M. Barani, M. R. Akbarizadeh, N. Pal Singh Chauhan, S. Jadoun, M. Dehghani Soltani and P. Zarrintaj, *Polymers*, 2022, **14**, 1259.
36 T. Saha, A. K. Bhowmick, T. Oda, T. Miyauchi and N. Fujii, *Polym. Degrad. Stab.*, 2016, **134**, 60–75.
37 M. Bai, B. Wilske, F. Buegger, J. Esperschutz, M. Bach, H. G. Frede and L. Breuer, *Environ. Sci. Pollut.*, 2015, **22**, 5444–5452.
38 D. Li, X. Guo, H. Du, W. Ding, M. Li and Y. Xu, *J. Mech. Behav. Biomed. Mater.*, 2023, **147**, 106144.
39 W. Ding, M. Chen, H. Du, X. Guo, H. Yuan, M. Li and Y. Xu, *Int. J. Biol. Macromol.*, 2024, **271**, 132530.
40 X. Zhao, J. Gao, H. Han, X. Lou, H. Ma, X. Su, L. Zhang, J. Tian, B. Lei and Y. Zhang, *Chem. Eng. J.*, 2023, **474**, 145609.
41 K. Cherednichenko, A. Sayfutdinova, D. Rimashevskiy, B. Malik, A. Panchenko, M. Kopitsyna, S. Ragnaev, V. Vinokurov, D. Voronin and D. Kopitsyn, *Polymers*, 2023, **15**, 3757.
42 W. Liu, T. Wang, C. Yang, B. W. Darvell, J. Wu, K. Lin, J. Chang, H. Pan and W. W. Lu, *Osteoporosis Int.*, 2016, **27**, 93–104.
43 D. H. Kohn, M. Sarmadi, J. I. Helman and P. H. Krebsbach, *J. Biomed. Mater. Res.*, 2002, **60**, 292–299.
44 K. Kato and M. Matsushita, *J. Bone Miner. Metab.*, 2014, **32**, 17–28.

Open Access Article. Published on 25 July 2024. Downloaded on 11/19/2025 6:58:59 AM.
This article is licensed under a Creative Commons Attribution-NonCommercial 3.0 Unported Licence.

45 O. Wahlstrom, C. Linder, A. Kalen and P. Magnusson, *Platelets*, 2007, **18**, 113–118.
46 P. Liang, J. Zheng, Z. Zhang, Y. Hou, J. Wang, C. Zhang and C. Quan, *J. Biomater. Sci., Polym. Ed.*, 2019, **30**, 34–48.
47 C. L. Salgado, B. I. B. Teixeira and F. J. M. Monteiro, *Front. Bioeng. Biotechnol.*, 2019, **7**, 206.
48 D. Bencivenga, A. Tramontano, A. Borgia, A. Negri, I. Caldarelli, A. Oliva, S. Perrotta, F. Della Ragione and A. Borriello, *Cell Cycle*, 2014, **13**, 3768–3782.
49 E. T. P. Bergamo, I. D. F. Balderrama, M. R. Ferreira, R. Spielman, B. V. Slavin, A. Torroni, N. Tovar, V. V. Nayak, B. R. Slavin, P. G. Coelho and L. Witek, *J. Biomed. Mater. Res., Part B*, 2023, **111**, 1966–1978.
50 T. Shen, W. Yang, X. Shen, W. Chen, B. Tao, X. Yang, J. Yuan, P. Liu and K. Cai, *ACS Biomater. Sci. Eng.*, 2018, **4**, 3211–3223.
51 Z. Geng, R. Dong, X. Li, X. Xu, L. Chen, X. Han, D. Liu and Y. Liu, *Int. J. Nanomed.*, 2024, **19**, 6427–6447.

 This journal is © The Royal Society of Chemistry 2024